High-Sensitivity Strain Gauge Based on a Single Wire of Gold Nanoparticles Fabricated by Stop-and-Go Convective Self-Assembly

Cosmin Farcau,[†] Neralagatta M. Sangeetha,[†] Helena Moreira,[†] Benoît Viallet,[†] Jérémie Grisolia,[†] Diana Ciuculescu-Pradines,[‡] and Laurence Ressier[†,*]

[†]Université de Toulouse, LPCNO, INSA-CNRS-UPS, 135 Avenue de Rangueil, Toulouse, 31077, France, and [‡]Université de Toulouse, Laboratoire de Chimie de Coordination (CNRS), 205 Route de Narbonne, Toulouse 31077, France

ABSTRACT High-sensitivity strain gauges based on single wires of close-packed 14 nm colloidal gold nanoparticles are obtained by a novel variant of convective self-assembly (CSA). This CSA mode named stop-and-go CSA enables the fabrication of nanoparticle wires only a few micrometers wide, separated by distances that can be easily tuned over tens to hundreds of micrometers. Nanoparticle wires are obtained in a single step by direct deposition of nanoparticles from suspensions onto flexible polyethylene terephthalate films, without any lithographic prepatterning. When connected between two electrodes, such single nanoparticle wires function as miniature resistive strain gauges. The high sensitivity, repeatability, and robustness demonstrated by these single-wire strain gauges make them extremely promising for integration into micro-electromechanical systems or for high-resolution strain mapping.

KEYWORDS: convective self-assembly · colloidal gold nanoparticles · flexible polymer substrate · strain gauge

The understanding of the unique properties of colloidal nanoparticles and their exploitation for the development of innovative functional devices is advancing rapidly.[1−4] Many of the emerging applications of colloidal nanoparticles are based on interparticle electronic, optic, or magnetic coupling effects in hierarchical assemblies comprising a large number of these.[5−8] One of the recent applications based on interparticle electronic coupling is sensing of strain.[9−13] Resistive strain gauges have been fabricated from assemblies of colloidal gold nanoparticles on flexible substrates. The high sensitivity of these devices is due to the exponential dependence of tunnel resistance on the separation between adjacent nanoparticles in the assembly.[14,15] The deposition of gold nanoparticles on flexible substrates was achieved by techniques such as airbrush spraying[11] and layer-by-layer deposition,[12] which yield large-area planar nanoparticle films. Recently, our group developed strain gauges made of arrays of parallel gold nanoparticle wires obtained by convective self-assembly (CSA) based on "stick−slip" mechanism, on flexible polyethylene terephthalate (PET) films, and demonstrated that 2D nanoparticle assemblies make more sensitive strain sensors than 3D ones.[13]

In this work, we report on the fabrication of the smallest strain sensors developed to date, which are based on single wires of 14 nm colloidal gold nanoparticles. These wires, a few micrometers wide, were made by a variant of CSA called stop-and-go convective self-assembly (SG-CSA), which we describe in this paper. The sensitivity of these strain gauges made of single nanoparticle wires was estimated under compressive and tensile bending for strain values in the range −0.8% to +0.8%. The repeatability of electrical response and the robustness of these miniature strain gauges under cyclic strain loading were also evaluated. Finally, uniaxial stretching was performed to assess the efficiency of these sensors at higher strain values (0−10%).

RESULTS AND DISCUSSION

Stop-and-Go Convective Self-Assembly. Convective self-assembly involves the translation of the meniscus of a drop of colloidal suspension across a substrate. Under adequate experimental conditions, particles in the colloidal suspension are deposited along the straight meniscus of the suspension drop due to particle flux toward the substrate−liquid−air contact line caused by solvent evaporation in this area.[16−20] A majority of literature reports deal with the convective self-assembly of large (hundreds of nanometers to few micrometers) colloids for

* Address correspondence to laurence.ressier@insa-toulouse.fr.

Received for review May 19, 2011 and accepted August 7, 2011.

Published online August 07, 2011
10.1021/nn201833y

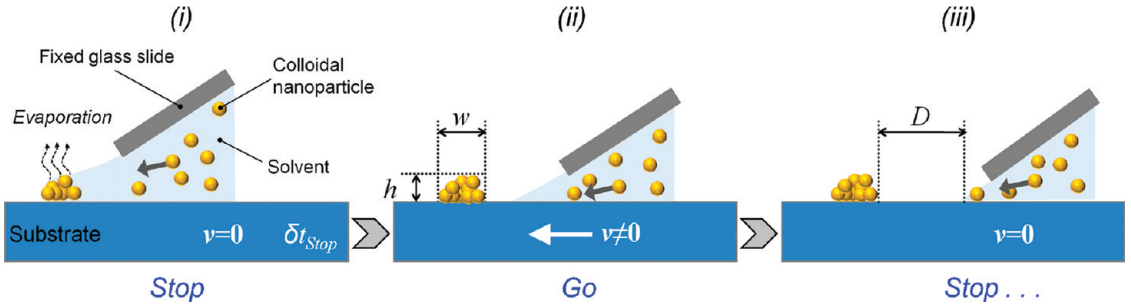

Figure 1. Principle of convective self-assembly in the stop-and-go mode: (i) the fast moving meniscus is stopped at the desired position and remains for a given time interval δt_{Stop}; (ii) the meniscus is translated with high speed *v*, leaving a deposited nanoparticle wire of width *w* and thickness *h*; (iii) the meniscus is stopped after a chosen distance *D*. This process can then be repeated as many times as required.

the fabrication of planar films.[19−22] Recently, a few groups have reported the creation of regular arrays of electrically conductive wires of ≤20 nm colloidal gold nanoparticles on rigid (Si, GaAs)[23−25] or flexible (PET)[13] substrates by CSA, thanks to the so-called stick−slip mechanism, which involves the periodic pinning and depinning of the moving meniscus.[23−27] The width and the thickness of the nanoparticle wires obtained by CSA operating in the stick−slip mode can be controlled by manipulating the substrate temperature and the meniscus translation speed. However, with the stick−slip motion, the distance between the nanoparticle wires cannot be controlled independently of the width and thickness of the wires.[22,27]

The new stop-and-go mode of CSA, which is presented here allows a precise control over the distance between nanoparticle wires by deliberate periodic triggering of the "stick" and "slip" steps. SG-CSA was implemented on a homemade CSA setup in horizontal configuration, in which the temperature of the substrate and its translation speed are regulated. In this variant of CSA, a straight meniscus is obtained by confining the colloidal suspension along the edge of a rectangular glass slide brought in the proximity of the substrate (Figure 1). The fast moving meniscus is deliberately stopped at a desired position on the substrate and confined there for a chosen time interval δt_{Stop} (Figure 1, step (i)). This represents the imposed stick step, during which particles form a linear deposit along the meniscus. The slip step is controlled by translating the meniscus at speeds *v*, 10−100 times larger than those at which the stick−slip mechanism operates (Figure 1, step (ii)). This high speed ensures that only the nanoparticle assembly formed during the meniscus dwelling is left on the substrate and avoids the formation of nanoparticle assemblies during meniscus translation. The meniscus may then be stopped at the next desired position (Figure 1, step (iii)), and the process can be repeated as many times as required. The width *w* and the thickness *h* of the fabricated nanoparticle wires are determined by the dwelling time δt_{Stop} and are interdependent. On the contrary, the distance *D* between the wires can be defined at will, independently of the wire cross-section. As in the stick−slip CSA, the length of nanoparticle wires can typically be several centimeters and is limited only by the physical dimensions of the substrate and the fixed glass slide. Moreover, SG-CSA can be applied on any kind of rigid or flexible, smooth, wettable substrates.

For the current work, 14 nm bis (*p*-sulfonatophenyl) phenylphosphine dihydrate dipotassium salt (BSPP) functionalized colloidal gold nanoparticles were used, and nanoparticle wires were fabricated by SG-CSA on flexible PET substrates. Optical microscopy images of three different arrays of wires are presented in Figure 2. The arrays in Figure 2a and b are both composed of nanoparticle wires separated by the same regular distance D = 0.05 mm and were obtained with the same v = 0.1 mm s^{-1}. The only difference between these two wire arrays is the dwelling time δt_{Stop} used during SG-CSA, which leads to nanoparticle wires of different lateral dimensions: the wires shown in Figure 2a obtained with a δt_{Stop} = 15 s, have a width $w = 6\ \mu$m and a thickness h = 55 nm, while those in Figure 2b, obtained with a δt_{Stop} = 30 s, have a width $w = 9\ \mu$m and a thickness h = 92 nm. The nanoparticle wires in Figure 2c were obtained under identical conditions to those in Figure 2b, and hence have the same geometry, but are separated by a distance D of 0.2 mm, chosen at will. The length of the wires is 1 cm in each case. These results prove that SG-CSA is indeed a powerful and flexible method that allows fabricating parallel nanoparticle wires separated by a tunable distance independently of their cross-section. There are only a few examples in the literature for fabricating wire-like assemblies of colloidal metal nanoparticles, with control over the internanoparticle wire distance. These are based on dip-coating[29,30] or more complex techniques such as nanomolding in capillaries.[31] Although programmed dip-coating appears rather promising, it does not provide as precise a control over the meniscus position as in the case of a colloidal droplet confined between the substrate and a deposition plate.

Closer inspections of the wires by scanning electron microscopy (Figure 3) reveal that in all cases the gold nanoparticles form a close-packed assembly inside the

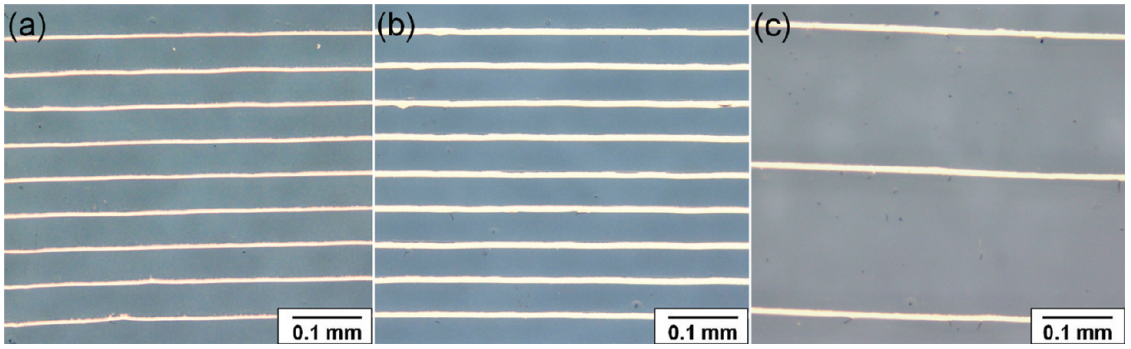

Figure 2. Optical microscopy images of arrays of identical parallel wires made of 14 nm gold nanoparticles using stop-and-go CSA: wires with a width $w = 6\ \mu$m (a) and $w = 9\ \mu$m (b), separated by the same distance $D = 0.05$ mm; wires with the same width $w = 9\ \mu$m, separated by a distance $D = 0.05$ mm (b) and $D = 0.2$ mm (c).

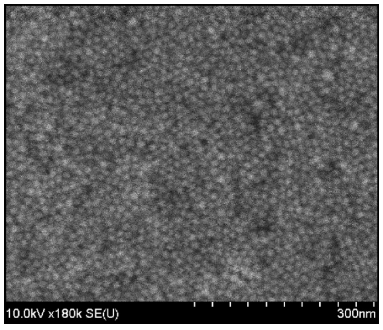

Figure 3. Scanning electron microscopy image of the packing of 14 nm gold nanoparticles forming the wires.

wires. The observed packing and organization are the same as observed for nanoparticle wires obtained by CSA based on stick–slip.[13]

Strain Gauge Fabrication. Single wires comprising 14 nm BSPP colloidal gold nanoparticles made by SG-CSA on PET substrates, similar to those presented in Figure 2c, were electrically connected by two gold electrodes to fabricate miniature resistive strain gauges. The electrodes, 50 nm thick and spaced by 50 μm, were made by stencil lithography to avoid any contamination of the nanoparticle assembly by resists or solvents used in photolithography.[23] An optical microscopy image of a typical resistive strain gauge based on a single nanoparticle wire is shown in Figure 4a. The active area of the sensor is marked by a rectangle, while the rest of the nanoparticle wire covered by the electrodes is blurred. The black lateral regions correspond to the drops of conductive epoxy glue used to connect copper wires to the external measurement devices.

A 3D atomic force microscopy (AFM) image of the active area of the nanoparticle strain gauge (marked by a white rectangle in Figure 4a) is presented in Figure 4b. The AFM cross-section in Figure 4c reveals that the nanoparticle wire constituting the active area of the sensor is multilayered, with the thickness gradually increasing from one edge to the other. This asymmetry is strictly related to the shape of the meniscus and the direction of its translation during SG-CSA: the wire starts to grow from its thin side, facing the dry region of the substrate. This profile is accentuated by the meniscus continuing to slowly move at the beginning of the dwelling time, due to a dynamic contact angle that is slightly smaller than the equilibrium one.[28] The 50 μm long nanoparticle wire shown in Figure 4 has a width w of 8 μm at the base and a maximum thickness h of 85 nm, leading to an active area of only 4×10^{-4} mm^2.

Electromechanical Response of Strain Gauges. Prior to testing the response of nanoparticle-based gauges to applied strain, their initial resistances R_0 were measured. The current *versus* voltage characteristics at room temperature were linear, yielding a resistance of $21 \times 10^6\ \Omega$ for the nanoparticle-based strain gauge presented in Figure 4. By taking into account the length of the nanoparticle wire constituting the active area of this strain sensor and its cross-sectional area deduced by AFM, the corresponding resistivity was estimated to be 0.2 $\Omega \cdot$m. This resistivity is about 7 orders of magnitude higher than that of bulk gold, suggesting that the BSPP capping layer of gold nanoparticles is indeed effective in imposing a significant tunnel barrier. It has been shown in several studies that the molecular capping layer is a crucial parameter for controlling the conductivity of nanoparticle films.[32] Transition from metallic to insulating behavior has been observed for nanoparticle films when the length of the bifunctional molecules cross-linking them was increased.[33] The tunnel barrier observed for BSPP molecules is consistent with that obtained for other molecules that yield comparable interparticle distances.[34]

In order to evaluate the performance of the fabricated nanoparticle-based strain gauges, variation of their electrical resistance ΔR was monitored in synchrony with the bending of the flexible PET substrate. The sensors were subjected to compressive and tensile strains by bending them over the inner and outer surfaces respectively, of cylindrical tubes of different diameters. The relative resistance variation $\Delta R/R_0$ as a function of applied strain ε, for the nanoparticle strain gauge shown in Figure 4 is presented in Figure 5

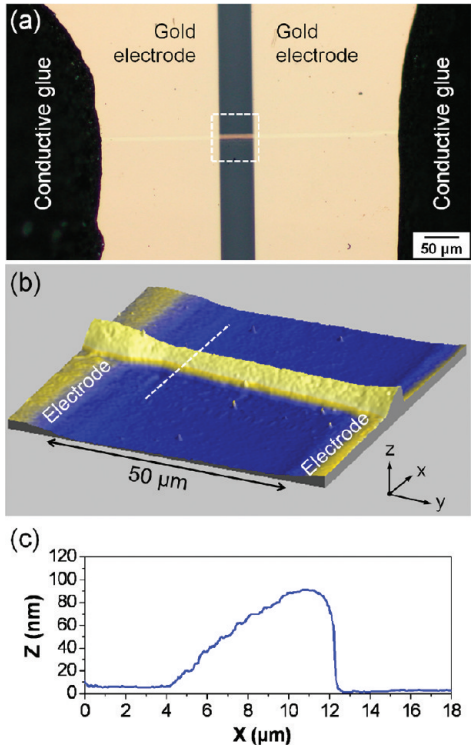

Figure 4. (a) Optical microscopy image of a typical resistive strain gauge based on a single wire of 14 nm gold nanoparticles. (b) AFM topographical image of the active area of the strain gauge (marked by a white rectangle in (a)). (c) AFM cross-section of the nanoparticle wire (marked by a white dashed line in (b)).

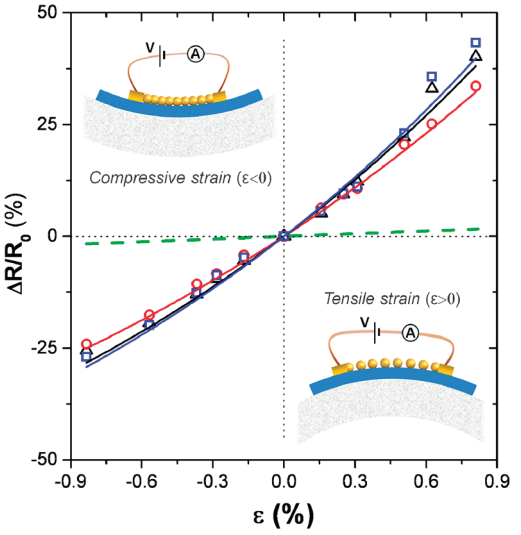

Figure 5. Relative resistance variation $\Delta R/R_0$ as a function of induced strain ε for three different nanoparticle-based strain gauges of similar morphology. Red circles correspond to the nanoparticle-based strain gauge presented in Figure 4. The solid lines are fits with the equation $\Delta R/R_0 = \exp(g\varepsilon) - 1$. The dashed green line corresponds to a conventional metal foil gauge with a gauge factor of 2. The insets show schemes of the nanoparticle-based strain gauge under compressive (left) and tensile (right) strain. For simplicity, only one nanoparticle layer is represented.

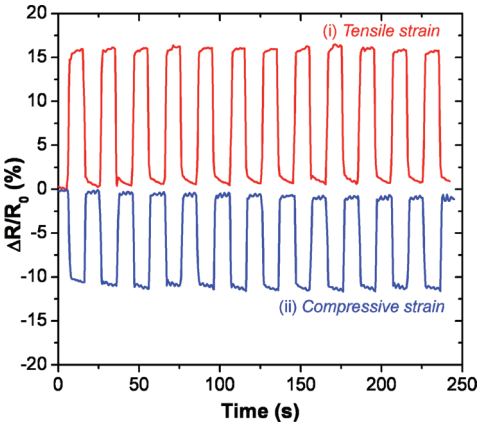

Figure 6. Time-dependent response of the nanoparticle-based strain gauge presented in Figure 4 and Figure 5 (red circles) undergoing a series of deformation cycles between (i) $\varepsilon = 0$ and $\varepsilon = 0.3\%$ and (ii) $\varepsilon = 0$ and $\varepsilon = -0.3\%$.

(red circles). The other two data sets (black triangles and blue squares) correspond to replicates of single wire strain sensors of similar morphology. An exponential dependence of $\Delta R/R_0$ on strain ε is observed, which is consistent with an exponential dependence of the interparticle tunnel resistance on the nanoparticle separation. The experimental $\Delta R/R_0$ *versus* ε curves can be well fitted with the equation $\Delta R/R_0 = \exp(g\varepsilon) - 1$ where g is a constant characterizing the sensitivity of the nanoparticle-based strain gauge. Similar responses observed for the replicates of similar morphology confirm the reproducibility of the SG-CSA fabrication process. For the examples presented in Figure 5 (continuous lines), $g = 35-41$, which makes the sensitivity of our miniature strain gauges comparable to those previously reported for strain gauges based on nanoparticle films extended over much larger areas.[11,12] Furthermore, these single nanoparticle wire strain gauges obtained by SG-CSA appear to be as sensitive as the ones comprising around 50 parallelly connected wires obtained by stick–slip CSA.[13] As seen in Figure 5, strain gauges based on single nanoparticle wires are very efficient under both tensile and compressive strains. However, the sensitivity of gauges is higher under tensile strain than under compressive strain due to the exponential dependence of relative resistance variation. The magnitude of relative resistance variation indicates that they are indeed much more sensitive than the conventional metal foil gauges and can reach the performances of the conventional semiconductor ones. For example, relative resistance variation of our nanoparticle-based strain gauge at 0.8% tensile strain is about 25 times higher than a conventional metal foil strain gauge with a typical gauge factor $G = (\Delta R/R_0)/\varepsilon$ of 2 (see dashed green line in Figure 5).

The physical robustness and the reliability of the single nanoparticle wire strain gauges were evaluated by subjecting them to a series of bending cycles under both compressive and tensile modes. For example, the

nanoparticle-based strain gauge presented in Figure 4 was bent and released repeatedly from 0 to ±0.3% strain values, at a frequency of one cycle each 20 s. The reproducible temporal dependence of its relative resistance variation is shown in Figure 6, indicating a stable response of the sensor with a very weak hysteresis. This result demonstrates that such strain gauges based on few micrometers wide single nanoparticle wires are robust enough to endure multiple bending cycles at strain values of ±0.3%. Apparently, the nanoparticle wire suffers no damage and produces a consistent electromechanical response at this strain loading. The cyclic responses at larger strain values (±0.6%) were however not completely reversible with a small progressive upward drift of the resistance at rest with each cycle, as compared to the initial resistance R_0.

Nanoparticle-based strain gauges made of multiple discrete entities are expected to withstand higher deformations without degradation than, for example, semiconductor ones. As strains accessible through our bending tests are restricted to absolute values < 0.8%, uniaxial stretching tests were performed to examine the response of single nanoparticle wire strain gauges up to a value of 10% tensile strain. Figure 7 presents characteristic curves for relative resistance variation along with the force applied on the PET substrate as a function of the strain. The curve for applied tensile force *versus* strain shows the two distinct regimes characteristic of polymer films: an elastic deformation regime (up to 2−3% strain in this case) followed by a plastic deformation one. The relative resistance variation $\Delta R/R_0$ increases with applied strain to more than 400% at a strain of 5% and starts to decrease with a further increase in strain. Interestingly, the response of the sensor follows pretty well the exponential law $\Delta R/R_0 = \exp(g\cdot\varepsilon) - 1$ up to about 3% strain, the region where the plastic deformation regime of the PET substrate begins. Beyond these strain values, when the substrate has entered the plastic deformation regime, the $\Delta R/R_0$ curve deviates from the exponential behavior. It then reaches a maximum and finally starts decreasing. The electrical response of the sensor in the plastic deformation regime can tentatively be attributed to the polymer deformation in the direction perpendicular to the stretching direction, which causes a decrease of the internanoparticle distances. This counterbalances the effect of elongational strain in the stretching direction, causing deviations from exponential behavior. It is noteworthy that the sensor responses to tensile strains by uniaxial stretching and bending are similar in magnitude over the range 0−0.8%. The maximum strain of 3% up to which the sensor follows the typical exponential behavior is much higher than the limit of deformation of semiconductor gauges and equals that of the metal foil ones. It appears that this strain value is limited by the mechanical properties of the PET substrate. In fact, even after an elongation of 10%, when the PET substrate has been irreversibly deformed, the single nanoparticle wire sustains its strain sensing capability and is able to detect compressive or tensile strain upon bending. Clearly, these results demonstrate the true potential of nanoparticle-based sensors, which not only match the sensitivity of semiconductor gauges but also withstand much higher strain values, without breaking.

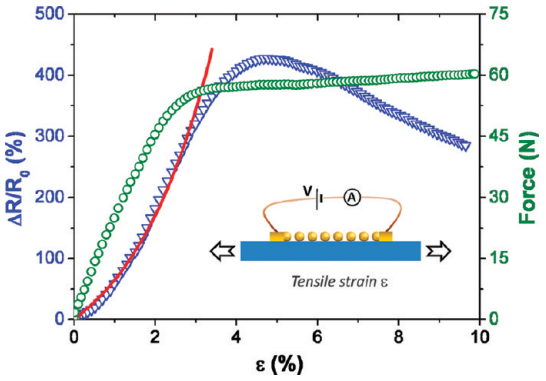

Figure 7. Relative resistance variation $\Delta R/R_0$ (blue triangles) and applied tensile force (green circles) as a function of induced strain ε for a single wire strain gauge, under uniaxial stretching. The red continuous line represents a fit of the experimental $\Delta R/R_0$ *versus* ε curve with the equation $\Delta R/R_0 = \exp(g\cdot\varepsilon) - 1$.

CONCLUSIONS

We have presented a variant of convective self-assembly, named stop-and-go CSA, which allowed the fabrication of miniature strain gauges based on single wires of 14 nm gold nanoparticles with an active area of only 4×10^{-4} mm^2, on PET substrates without any lithography patterning. The sensitivity of these nanoparticle-based strain gauges, which are of the smallest dimensions developed so far, is more than 1 order of magnitude higher than that of the conventional metal foil gauges and approaches that of semiconductor ones. Their electromechanical response was reproduced with replicate samples, and these strain gauges based on single nanoparticle wires, a few micrometers wide, are robust enough to withstand both compressive and tensile cyclic strain loading. Moreover, uniaxial stretching tests prove that these nanoparticle-based strain gauges can function in accordance with exponential laws up to about 3% strain, and this value appears to be limited by the mechanical properties of the PET substrate. This value is much higher than the limit of deformation of semiconductor gauges and equals that of the metal foil ones.

These highly sentivitive, miniature strain gauges based on single nanoparticle wires could have a wide

range of applications. For example, they could be integrated into miniature devices such as microelectromechanical systems. Since SG-CSA also allows patterning regular arrays of nanoparticle wires, it facilitates the reliable fabrication of arrays of strain gauges based on single wires of nanoparticles, which could be very useful in mapping strain with unprecedented spatial resolution. In a more general perspective, the capabilities of SG-CSA to fabricate arrays of nanoparticle wires on flexible or rigid surfaces with a fine control on the array period independently of the lateral wire dimensions offer ample opportunities for the bottom-up development of other innovative nanoparticle-based devices.

METHODS

Synthesis and Functionalization of Colloidal Gold Nanoparticles. Gold nanoparticles of 14 ± 1 nm were synthesized by the reduction of tetrachloroauric acid by sodium citrate in aqueous phase using the standard Turkevich method.[35] The citrate-stabilized particles were refluxed overnight with bis (*p*-sulfonatophenyl) phenylphosphine dihydrate dipotassium salt (BSPP) to facilitate ligand exchange.[36] The BSPP ligand was used because it confers long-term stability to the gold colloids at the relatively high concentrations required for CSA and also serves as an adequate tunnel barrier between assembled nanoparticles. The BSPP-capped gold nanoparticles were purified by repeated precipitation with ethanol and finally redispersed in deionized water to a final concentration of ~0.004% vol.

Stop-and-Go Convective Self-Assembly. The homemade CSA deposition system is based on a glass deposition plate placed in the vicinity (250 μm) of the horizontal substrate, at an angle of 30° (Figure 1). The substrate is fixed on a copper plate, which was maintained at a temperature of 27 °C in this study. A 20 μL droplet of colloidal suspension is injected into the wedge formed by the deposition plate and the substrate. The meniscus formed by the colloidal suspension with the substrate is dragged across the substrate by translating the latter at speeds v ranging from 50 nm/s to 1 mm/s. Computer software allows programming the periodic movement and stopping of the substrate. This CSA setup is mounted under an Olympus BXFM optical microscope to allow real-time observations. In the present study, 125 μm thick PET films were used as substrates. Before SG-CSA experiments, these films were briefly cleaned with acetone, rinsed with ultrahigh-quality water, and dried in a stream of nitrogen followed by ultraviolet treatment for 5 min. This rendered them hydrophilic, with low contact angles between 15° and 20°. The nanoparticle wires fabricated by SG-CSA on PET films were obtained at an ambient temperature of 25 °C (samples in Figure 2) and 23 °C (sample in Figure 4) and a relative humidity of 45−48%.

Characterization by Microscopy. The fabricated nanoparticle wires and the associated strain gauges were observed by optical microscopy (Olympus BXFM), atomic force microscopy in tapping mode (Multimode Nanoscope IIIA from Veeco Instruments), and scanning electron microscopy (Hitachi S-4800).

Electromechanical Tests. Prior to testing the response of nanoparticle-based gauges to applied strain, current *versus* voltage curves of the strain gauges were measured within ±1 V range at room temperature. Their electrical resistance variations ΔR under a constant voltage of 0.5 V were then monitored in synchrony with the bending of the PET substrates. To test the gauges both under compressive and tensile strains, the PET substrates were placed in conformational contact with the inner and outer surfaces of various cylindrical tubes of known diameters (see insets of Figure 5). The strain induced in the single nanoparticle wires was determined from the tube diameter d and the substrate thickness H by $\varepsilon = \pm(H/(d \pm H))$, with the plus and minus signs representing tensile and compressive strains, respectively. A Deben Microtest tensile unit was used to perform pure uniaxial stretching tests, to explore higher strain values up to 10%. The strain gauges used for these tests were prepared on dumbbell-shaped PET substrates.

Acknowledgment. This work was supported by the French National Agency (ANR) in the frame of its program "Recherche Technologique Nano-INNOV/RT" (NANOCOMM project no. ANR-09-NIRT-004).

REFERENCES AND NOTES

1. Steckel, J. S.; Snee, P.; Coe-Sullivan, S.; Zimmer, J. P.; Halpert, J. E.; Anikeeva, P.; Kim, L.; Bulovic, V.; Bawendi, M. G. Color-Saturated Green-Emitting QD-LEDs. *Angew. Chem., Int. Ed.* **2006**, *45*, 5796–5799.
2. Talapin, D. V.; Murray, C. B. PbSe Nanocrystal Solids for n- and p-Channel Thin Film Field-Effect Transistors. *Science* **2005**, *310*, 86–89.
3. Millstone, J. E.; Hurst, S. J.; Métraux, G. S.; Cutler, J. I.; Mirkin, C. A. Colloidal Gold and Silver Triangular Nanoprisms. *Small* **2009**, *5*, 646–664.
4. Jarosz, M. V.; Porter, V. J.; Fisher, B. R.; Kastner, M. A.; Bawendi, M. G. Photoconductivity Studies of Treated CdSe Quantum Dot Films Exhibiting Increased Exciton Ionization Efficiency. *Phys. Rev. B* **2004**, *70*, 195327.
5. Nakanishi, H.; Bishop, K. J. M.; Kowalczyk, B.; Nitzan, A.; Weiss, E. A.; Tretiakov, K. V.; Apodaca, M. M.; Klajn, R.; Stoddart, J. F.; Grzybowski, B. A. Photoconductance and Inverse Photoconductance in Films of Functionalized Metal Nanoparticles. *Nature* **2009**, *460*, 371–375.
6. Krasteva, N.; Besnard, I.; Guse, B.; Bauer, R. E.; Müllen, K.; Yasuda, A.; Vossmeyer, T. Self-Assembled Gold Nanoparticle/Dendrimer Composite Films for Vapor Sensing Applications. *Nano Lett.* **2002**, *2*, 551–555.
7. Li, S.; Liu, H.; Liu, L.; Tian, L.; He, N. A Novel Automated Assay with Dual-Color Hybridization for Single-Nucleotide Polymorphisms Genotyping on Gold Magnetic Nanoparticle Array. *Anal. Biochem.* **2010**, *405*, 141–143.
8. Kasyutich, O.; Desautels, R. D.; Southern, B. W.; van Lierop, J. Novel Aspects of Magnetic Interactions in a Macroscopic 3D Nanoparticle-Based Crystal. *Phys. Rev. Lett.* **2010**, *104*, 127205.
9. Murugaraj, P.; Mainwaring, D.; Khelil, N. A.; Peng, J. L.; Siegele, R.; Sawant, P. The Improved Electromechanical Sensitivity of Polymer Thin Films Containing Carbon Clusters Produced in situ by Irradiation with Metal Ions. *Carbon* **2010**, *48*, 4230–4237.
10. Lim, M. A.; Lee, Y. W.; Han, S. W.; Park, I. Novel Fabrication Method of Diverse One-Dimensional Pt/ZnO Hybrid Nanostructures and its Sensor Application. *Nanotechnology* **2011**, *22*, 035601.
11. Herrmann, J.; Muller, K.; Reda, T.; Baxter, G. R.; Raguse, B.; de Groot, G. J. J. B.; Chai, R.; Roberts, M.; Wieczorek, L. Nanoparticle Films as Sensitive Strain Gauges. *Appl. Phys. Lett.* **2007**, *91*, 183105.
12. Vossmeyer, T.; Stolte, C.; Ijeh, M.; Kornowski, A.; Weller, H. Networked Gold-Nanoparticle Coatings on Polyethylene: Charge Transport and Strain Sensitivity. *Adv. Funct. Mater.* **2008**, *18*, 1611–1616.
13. Farcau, C.; Moreira, H.; Viallet, B.; Grisolia, J.; Ciuculescu-Pradines, D.; Amiens, C.; Ressier, L. Monolayered Wires of Gold Colloid Nanoparticles for High-Sensitivity Strain Sensing. *J. Phys. Chem. C* **2011**, *115*, 14494–14499.
14. Parthasarathy, R.; Lin, X.; Jaeger, H. Electronic Transport in Metal Nanocrystal Arrays: The Effect of Structural Disorder on Scaling Behavior. *Phys. Rev. Lett.* **2001**, *87*, 186807.
15. Wuelfing, W. P.; Green, S. J.; Pietron, J. J.; Cliffel, D. E.; Murray, R. W. Electronic Conductivity of Solid-State, Mixed-Valent, Monolayer-Protected Au Clusters. *J. Am. Chem. Soc.* **2000**, *122*, 11465–11472.

16. Dimitrov, A. S.; Nagayama, K. Steady-State Unidirectional Convective Assembling of Fine Particles into Two-Dimensional Arrays. *Chem. Phys. Lett.* **1995**, *243*, 462–468.
17. Prevo, B. G.; Kuncicky, D. M.; Velev, O. D. Engineered Deposition of Coatings from Nano- and Micro-particles: A Brief Review of Convective Assembly at High Volume Fraction. *Colloid Surf. A* **2007**, *311*, 2–10.
18. Kraus, T.; Malaquin, L.; Delamarche, E.; Schmid, H.; Spencer, N. D.; Wolf, H. Closing the Gap between Self-Assembly and Microsystems Using Self-Assembly, Transfer, and Integration of Particles. *Adv. Mater.* **2005**, *17*, 2438–2442.
19. Kim, M. H.; Im, S. H.; Park, O. O. Rapid Fabrication of Two- and Three-Dimensional Colloidal Crystal Films via Confined Convective Assembly. *Adv. Funct. Mater.* **2005**, *15*, 1329–1335.
20. Jiang, P.; Bertone, J. F.; Hwang, K. S.; Colvin, V. L. Single-Crystal Colloidal Multilayers of Controlled Thickness. *Chem. Mater.* **1999**, *11*, 2132–2140.
21. Chen, K.; Stoianov, S. V.; Bangerter, J.; Robinson, H. D. Restricted Meniscus Convective Self-Assembly. *J. Colloid Interface Sci.* **2010**, *344*, 315–320.
22. Ding, T.; Song, K.; Clays, K.; Tung, C. Fabrication of 3D Photonic Crystals of Ellipsoids: Convective Self-Assembly in Magnetic Field. *Adv. Mater.* **2009**, *21*, 1936–1940.
23. Grisolia, J.; Viallet, B.; Amiens, C.; Baster, S.; Cordan, A. S.; Leroy, Y.; Soldano, C.; Brugger, J.; Ressier, L. 99% Random Telegraph Signal-Like Noise in Gold Nanoparticle μ-Stripes. *Nanotechnology* **2009**, *20*, 355303.
24. Farcau, C.; Moreira, H.; Viallet, B.; Grisolia, J.; Ressier, L. Tunable Conductive Nanoparticle Wire Arrays Fabricated by Convective Self-Assembly on Non-patterned Substrates. *ACS Nano* **2010**, *4*, 7275–7282.
25. Kakefuda, Y.; Narita, K.; Komeda, T.; Yoshimoto, S.; Hasegawa, S. Synthesis and Conductance Measurement of Periodic Arrays of Gold Nanoparticles. *Appl. Phys. Lett.* **2008**, *93*, 163103.
26. Watanabe, S.; Inukai, K.; Mizuta, S.; Miyahara, M. T. Mechanism for Stripe Pattern Formation on Hydrophilic Surfaces by Using Convective Self-Assembly. *Langmuir* **2009**, *25*, 7287–7295.
27. Ray, M. A.; Kim, H.; Jia, L. Dynamic Self-Assembly of Polymer Colloids to Form Linear Patterns. *Langmuir* **2005**, *21*, 4786–4789.
28. Kumar, G.; Prabhu, K. N. Review of Non-Reactive and Reactive Wetting of Liquids on Surfaces. *Adv. Colloid Interf. Sci.* **2007**, *133*, 61–89.
29. Huang, J.; Fan, R.; Connor, S.; Yang, P. One-Step Patterning of Aligned Nanowire Arrays by Programmed Dip Coating. *Angew. Chem., Int. Ed.* **2007**, *46*, 2414–2417.
30. Diao, J. J.; Cao, Q. Gold nanoparticle wire and Integrated Wire Array for Electronic Detection of Chemical and Biological Molecules. *AIP Adv.* **2011**, *1*, 012115.
31. Duan, X.; Park, M.; Zhao, Y.; Berenschot, E.; Wang, Z.; Reinhoudt, D. N.; Rotello, V. M.; Huskens, J. Metal Nanoparticle Wires Formed by an Integrated Nanomolding–Chemical Assembly Process: Fabrication and Properties. *ACS Nano* **2010**, *4*, 7660–7666.
32. Zabet-Khosousi, A.; Dhirani, A. Charge Transport in Nanoparticle Assemblies. *Chem. Rev.* **2008**, *108*, 4072–4124.
33. Zabet-Khosousi, A.; Trudeau, P.; Suganuma, Y.; Dhirani, A.; Statt, B. Metal to Insulator Transition in Films of Molecularly Linked Gold Nanoparticles. *Phys. Rev. Lett.* **2006**, *96*, 156403.
34. Musick, M. D.; Keating, C. D.; Lyon, L. A.; Botsko, S. L.; Peña, D. J.; Holliway, W. D.; McEvoy, T. M.; Richardson, J. N.; Natan, M. J. Metal Films Prepared by Stepwise Assembly. 2. Construction and Characterization of Colloidal Au and Ag Multilayers. *Chem. Mater.* **2000**, *12*, 2869–2881.
35. Turkevich, J.; Stevenson, P. C.; Hillier, J. A Study of the Nucleation and Growth Processes in the Synthesis of Colloidal Gold. *Discuss. Faraday Soc.* **1951**, *11*, 55–75.
36. Loweth, C. J.; Caldwell, W. B.; Peng, X.; Alivisatos, A. P.; Schultz, P. G. DNA-Based Assembly of Gold Nanocrystals. *Angew. Chem., Int. Ed.* **1999**, *38*, 1808–1812.